Friction **11**(5): 704–715 (2023)
https://doi.org/10.1007/s40544-022-0647-0
ISSN 2223-7690
CN 10-1237/TH
RESEARCH ARTICLE

Load and velocity boundaries of oil-based superlubricity using 1,3-diketone

Yuyang YUAN[1,2], Tobias AMANN[3], Yuwen XU[1,2], Yan ZHANG[1,2], Jingfu CHEN[1,2], Chenqing YUAN[1,2], Ke LI[1,2,*]

[1] *School of Transportation and Logistics Engineering, Wuhan University of Technology, Wuhan 430063, China*

[2] *Reliability Engineering Institute, National Engineering Research Center for Water Transport Safety, MOST, Wuhan 430063, China*

[3] *Fraunhofer Institute for Mechanics of Materials IWM, Freiburg 79108, Germany*

Received: 23 January 2022 / Revised: 17 March 2022 / Accepted: 04 May 2022

Abstract: The clarification of the critical operating conditions and the failure mechanism of superlubricity systems is of great significance for seeking appropriate applications in industry. In this work, the superlubricity region of 1,3-diketone oil EPND (1-(4-ethyl phenyl) nonane-1,3-dione) on steel surfaces was identified by performing a series of ball-on-disk rotation friction tests under various normal loads (3.5–64 N) and sliding velocities (100–600 mm/s). The result shows that beyond certain loads or velocities superlubricity failed to be reached due to the following negative effects: (1) Under low load (≤ 3.5 N), insufficient running-in could not ensure good asperity level conformity between the upper and lower surfaces; (2) the high load (≥ 64 N) produced excessive wear and big debris; (3) at low velocity (≤ 100 mm/s), the weak hydrodynamic effect and the generated debris deteriorated the lubrication performance; (4) at high velocity (≥ 500 mm/s), oil migration occurred and resulted in oil starvation. In order to expand the load and velocity boundaries of the superlubricity region, an optimized running-in method was proposed to avoid the above negative effects. By initially operating a running-in process under a suitable combination of load and velocity (e.g. 16 N and 300 mm/s) and then switching to the target certain higher or lower load/velocity (e.g. 100 N), the superlubricity region could break through its original boundaries. The result of this work suggests that oil-based superlubricity of 1,3-diketone is a promising solution to friction reduction under suitable operating conditions especially using a well-designed running-in strategy.

Keywords: macroscopic superlubricity; 1,3-diketone oil; running-in process; load and velocity boundaries

1 Introduction

Since the concept of "superlubricity" was first proposed by Hirano and Shinjo using theoretical calculations in the early 1900s [1, 2], this novel lubrication state with the coefficient of friction (COF) smaller than 0.01 has been considered as an attractive technique to significantly improve energy efficiency and service life of mechanical devices [3]. Over the last three decades, various lubricants that possess superlubricity properties have been developed [4–8]. However, the tribological performance of a lubricant is a systematic behavior dependent on its operating conditions. In the so far reported superlubricity systems achieved using different testing equipment from atomic force microscope (AFM) to macroscopic tribometers, the normal load varies from the Nanonewton [9] to the Newton [10] level and the sliding velocity varies from the Nanometer per second [11] to the Meter per second level [12]. Therefore, it is necessary to clarify the critical operating conditions of these various superlubricity systems, understand the failure mechanism and explore the possible method for further improvement. This is of great significance for this novel technology to

* Corresponding author: Ke LI, E-mail: li_ke@whut.edu.cn

pertinently select suitable applied objects and promote its development to industrial applications.

For macroscopic superlubricity systems, a running-in process is necessary in most cases to promote a well-coordinated state of the lubricating materials and friction pairs [4, 13–22]. However, both too large or too small normal loads and sliding velocities would cause the failure of reaching superlubricity. For instance, water-based superlubricity using phosphoric acid (H_3PO_4) solution on Si_3N_4/glass surfaces has been widely studied [18, 23–25]. During the running-in process, a silica layer formed via the tribochemical reaction between water and Si_3N_4 can efficiently separate rubbing surfaces and provide a composite hydration layer with ultralow shear strength. Further studies investigated the degeneration process of the superlubricity state and revealed the failure mechanism under various loads and velocities [14, 16, 26]. At the low speed, the hydrodynamic effect of lubricating liquids is not strong enough to completely separate the tribopair surfaces. Under the low load, the insufficient running-in process needs a much longer time to achieve superlubricity. When the load or velocity is too high, severe wear accompanied by serious surface damage and abrasive particles results in superlubricity failure.

Besides water-based superlubricity, the friction minimization of oil-based materials, especially on metallic substrates, is also very desirable as oils and greases are still the most popular lubricating materials in industry [27]. In our prior work [19, 28–33], a synthetic oil 1,3-diketone with superlubricity on steel surfaces has been explored. Similar to the tribochemical reaction on glass surfaces using phosphoric acid solution, the explored diketone could also react with steel surfaces activated by the rubbing process, which eliminates direct solid contacts and generates a strongly adsorbed layer on surfaces; on the other hand, the rod-like molecular structure of diketone, similar to liquid crystals, facilitates the molecular alignment and the shear stress reduction of lubricating fluids. Although 1,3-diketone is considered to be a promising lubricant for industrial bearings or gears, the critical operating conditions of its superlubricity performance need to be deeply investigated.

By performing a series of ball-on-disk rotation friction tests under various normal loads and sliding velocities, this work aims to identify the superlubricity region of 1,3-diketone oil. Its failure mechanisms of superlubricity performance under different operating conditions were investigated through analysis of the morphology of worn surfaces, the chemical change of lubricating oil, and the generated wear debris after the friction tests. Furthermore, based on the discovered failure mechanism, the corresponding method for expanding its superlubricity region has been studied as well.

2 Materials and methods

As one of the most studied 1,3-diketone before, 1-(4-ethyl phenyl) nonane-1,3-dione (EPND, Fig. 1),

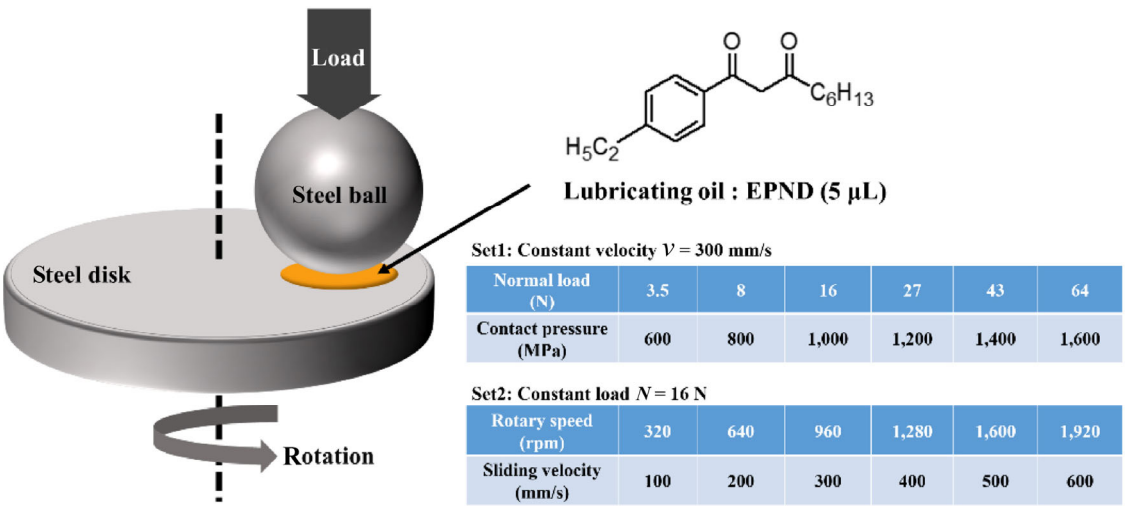

Set1: Constant velocity V = 300 mm/s

Normal load (N)	3.5	8	16	27	43	64
Contact pressure (MPa)	600	800	1,000	1,200	1,400	1,600

Set2: Constant load N = 16 N

Rotary speed (rpm)	320	640	960	1,280	1,600	1,920
Sliding velocity (mm/s)	100	200	300	400	500	600

Fig. 1 Two sets of ball-on-disk rotary friction tests using EPND lubricating oil.

synthesized via a Claisoen condensation reaction [29], was selected as the lubricating oil for the friction tests in this study. Steel (GB GCr15, i.e. DIN 100Cr6) balls (diameter = 12.7 mm, Sa = 0.03 μm, Sz = 0.13 μm) and disks (diameter = 20 mm, height = 20 mm, Sa = 0.14 μm, Sz = 2.47 μm) were used as the rotary friction pairs performed by a Multi-Functional Tribometer (MFT5000, Rtec-Instruments) at 25 °C. Before the test, one drop of EPND (5 μL) was placed on the disk, and the radius of the sliding track was kept constant (3 mm).

To discover the effect of normal load and sliding velocity separately, the friction tests were divided into two sets. In Set 1, six tests were performed at a constant velocity of 300 mm/s, but under various applied loads from 3.5 to 64 N, providing an initial contact pressure from 600 to 1,600 MPa. As for Set 2, under the same load of 16 N, six tests were carried out at different rotation speeds varied from 320 to 1,920 rpm, corresponding to the linear velocity from 100 to 600 mm/s. Each friction test was repeated three times to ensure data repeatability.

After the friction test, the worn morphology of steel specimens were examined by a laser scanning confocal microscope (LSCM, VK-X1000, Keyence). The chemical composition and wear debris in the resulting oil were analyzed by FTIR and LSCM respectively. For FTIR analysis, the resulting oil on the steel disk was directly collected by a capillary glass tube. Its FTIR spectra was recorded using a spectrometer (Nicolet6700, ThermoElectron Scientific Instruments) in the range of 4,000–450 cm^{-1} at a resolution of 4 cm^{-1}. For wear debris measurement, all resulting oil was flushed using ethanol from the disk into a beaker, and then diluted to be an ethanol solution with about 5 wt% of oil. After the ultrasonication for 5 min to ensure the well distribution of the abrasive particles, 1 μL solution was dropped on a glass slide and observed using LSCM.

3 Results and discussion

3.1 Effect of normal load

The load-carrying capacity is a key factor for lubricating oils to select the appropriate lubrication system in practical applications. Figure 2(a) displays the COF evolution under six different loads with the same constant velocity of 300 mm/s. In all tests COFs obviously decreased with the testing time, but superlubricity could only be achieved under the load between 8 and 43 N. When the load was 3.5 and 64 N, the resulting COFs were in the range of 0.013 to 0.016 at the end of the test. This result implies that the superlubricity performance strongly depends on normal loads. 3.5 and 64 N are the critical values of low load boundary and high load boundary respectively in the studied lubrication system. According to the optical images of wear surfaces measured by the laser microscope (Figs. S1 and S2 in the Electronic Supplementary Material (ESM)), the WSD (wear scar diameter) on balls, the WTW (wear track width) on disks are summarized together with the resulting COF values in Fig. 2(b). Based on the WSD, the resulting nominal pressures between the surfaces were 7, 13, 24, 35, 43, and 57 MPa under the six different loads respectively.

In addition, it shows that the WSD on the ball was always larger than the WTW on its corresponding disk. On one hand, due to the elastic deformation, the contact pressure distribution is elliptical with the maximum pressure at the contact center [34]. So the

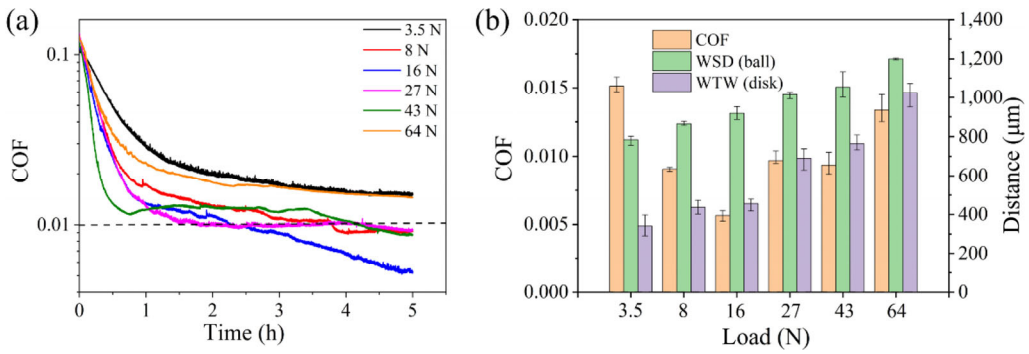

Fig. 2 (a) COF evolution and (b) resulting COF, WSD, and WTW values in the friction tests under various loads.

wear in the center of the worn area would be more noticeable than the edge after unloading. On the other hand, the contact region of the ball never changed during the rotary test, but the contact region of the disk kept changing with rotation during the whole testing time, i.e. the ball suffered a longer sliding distance than the single point of the disk. So the very shallow wear track on the disk was difficult to be observed [35]. With the help of 2D images in Fig. S2 in the ESM the boundary of the wear track was determined to depict the surface geometric profiles (Fig. 3). It can be found that the wear tracks of steel disks did not show obvious "hollow", which suggests that the running-in process in this study did not induce obvious surface conformity in the waviness level. However, it has been reported that the running-in process can also enhance the conformity in the asperity level by reducing the roughness of the two contact surfaces [36], and this degree of surface matching is so-called "asperity level conformity" [37, 38]. Thus the roughness of the wear scar on the ball, and the inside/outside area of the wear track on the disk (the detected area was 300 μm × 300 μm) in Figs. S1 and S2 in the ESM was measured, and the obtained Sa values were shown in Fig. 3. It suggests that the surface roughness of the ball was very small and kept nearly constant around 28 nm under different loads, which was similar to its original roughness of 30 nm. However, as the original disk was very rough (Sa = 140 nm), the roughness of the wear track was obviously reduced especially under high load, indicating the flattening of the asperities during the running-in process. In addition, the higher load not only decreased the roughness inside the wear track, but also increased the width of the observed wear track, which suggests that more area was involved in the wear process and resulted in lower discrepancy between WTW and WSD. So a higher WTW/WSD ratio could be used to represent better surface conformity after the friction test.

As its tribochemical reaction with iron is a key feature of EPND's superlubricity behavior, it is necessary to make a careful oil analysis after the friction test. Compared to the light-yellow color of pure EPND, Fig. 4(a) shows that EPND turned to red color especially under high loads. Our previous study has found that this kind of color change is from the generated iron chelate complex with EPND [29], and the FTIR spectra in Fig. 4(b) confirmed this point again for the oil samples in this study. For the pure EPND before the friction test, the strong absorption band at 1,609 cm^{-1} is assigned to the in-plane vibrations of O–H bond in the enol form. For the iron complex generated by the tribochemical reaction during the friction test, the signal at 1,581 cm^{-1} and absorption bands between 1,545 and 1,500 cm^{-1} are related to C=O and C=C stretch vibrations. Thus, by comparing the signal intensity of EPND and iron complex in Fig. 4(b), it suggests that the content of iron complex in the resulting oil after the friction test increased with the increasing testing load, which is consistent with the oil color gradient in Fig. 4(a). By comparing the absorption intensity of the characteristic peaks with the pure iron complex [29], the iron complex contents in all resulting oil were lower than 10%, indicating negligible viscosity variation during the friction tests according to our prior work [39].

In addition to the change in color, more and more black wear debris appeared in the oil as the load increased. From optical microscopy (Fig. 5) observation,

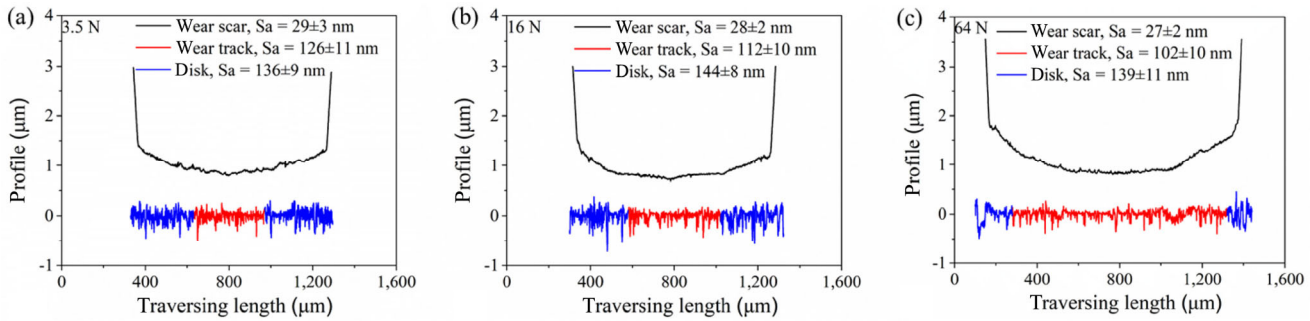

Fig. 3 Surface geometric profiles of the balls and the disks after the friction tests under various loads: (a) 3.5, (b) 16, and (c) 64 N.

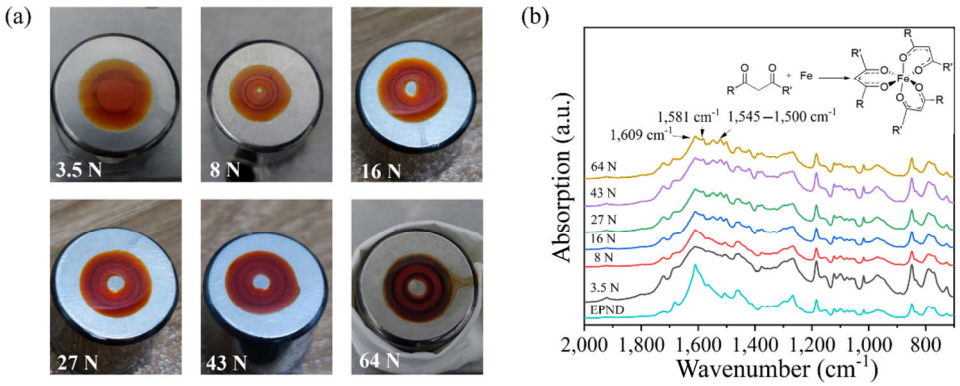

Fig. 4 (a) Photos of the resulting oil on steel disks and (b) FTIR spectra of pure EPND and the resulting oil after the friction tests under various loads.

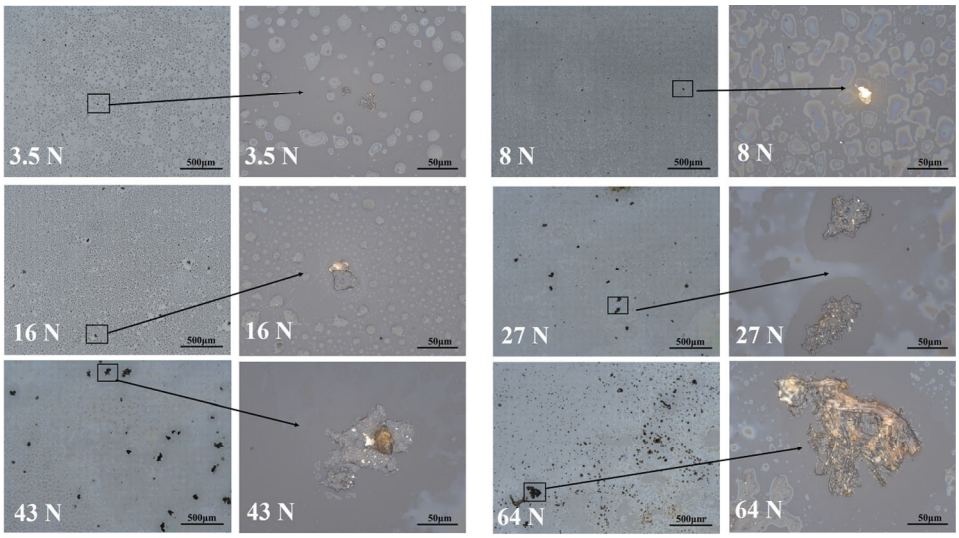

Fig. 5 Wear debris in the resulting oil after the friction tests under various loads.

both the amount and the size of wear debris in the resulting oil increased with the load. Notably, the maximum particle size in all oil samples was smaller than 100 μm except the one after the friction test under 64 N, in which the abrasive particle larger than 200 μm was observed.

Changes in the morphology of sliding surfaces, the chemical composition of oil and the formation of wear debris mentioned above are all closely related to the wear mechanism and the wear rate during the running-in process [40, 41]. In the lubrication system of EPND on steel surfaces, mechanical wear and tribochemical wear exist simultaneously, both of which strongly depends on the normal load. Figure 6 depicts the frictional force evolution in the friction tests under various loads. When the lowest load of 3.5 N was applied, the low severity of asperity

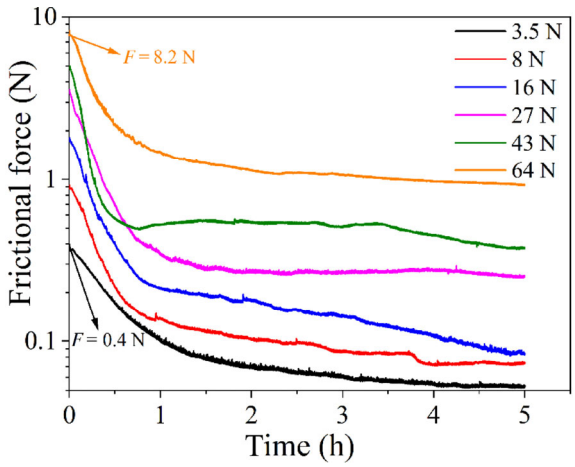

Fig. 6 Frictional force evolution in the friction tests under various loads.

contacts and collisions not only limited the abrasive wear [42] but also lowered the shear stress as the

initial frictional force was only 0.4 N, which could not supply enough energy for the tribochemical reaction [43]. So in such a case, the total wear was slight and the surface conformity was insufficient, which did not lead to superlubricity. When the load was moderately increased into the range of 8–43 N, superlubricity could be achieved on the larger and more conformal worn surfaces. However, it is worth noting that the increasing load and frictional force also elevated the ratio of mechanical wear against tribochemical wear. When the load was increased to 64 N, in the presence of severe mechanical wear the tribochemical reaction could not adopt the majority worn steel in the form of oil-soluble iron complex anymore. The significant amount of generated large abrasive particles induced terrible three-body wear [44] and finally resulted in the failure of superlubricity.

Since running-in under a suitable normal load can produce moderate wear and avoid excessive wear debris, a two-stage running-in process (Fig. 7(a)) is proposed to overcome the problems when the load is too low or too high. At first, the friction test was operated under a load of 16 N for 3 h to achieve superlubricity. Then the load was switched to the target load. In the case of reducing the load to 3.5 N, superlubricity was maintained with an even lower COF of 0.004, which suggests that the already established conformal surfaces (Fig. 7(b) and Fig. S3 in the ESM) were the key for superlubricity. In the case of elevating the load to 64 N, superlubricity failed with a rise of COF to 0.06. However, since the contact pressure has already been reduced in the first-stage running-in process, the initial frictional force at the switch point was only 3.8 N, which was much lower than the case of the friction test directly operated under 64 N (F = 8.2 N in Fig. 6). Then the superlubricity was recovered within a very short second-stage running-in process around 1.5 h. In this situation, the resulting nominal contact pressure in the superlubricity state was 67 MPa, which was higher than the case of 43 MPa achieved under 43 N in Fig. 2. Moreover, abrasive particles observation (Fig. 8) verified that this two-stage running-in process effectively avoided big wear debris and their deterioration to the lubrication performance.

3.2 Effect of sliding velocity

Besides the normal load, the sliding velocity is another significant parameter which strongly affects the hydrodynamic effect and film formation of lubricating oils. Figure 9(a) shows the COF evolution at six different velocities with the same constant load of 16 N. When the velocity was in the range of 200–400 mm/s, the superlubricity state was achieved after a running-in period of fewer than 3 h and remained stable through the rest of the experimental period. At the low velocity of 100 mm/s, the COF decreased very slowly and finally reached 0.022 at the end of the test. For the high velocity of 500 mm/s, the rapidly descending

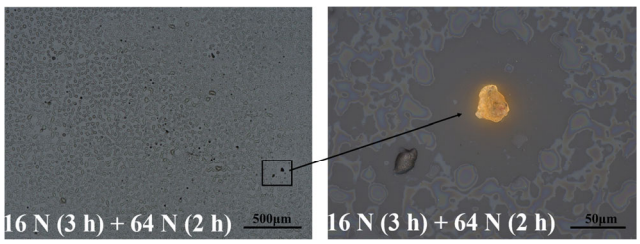

Fig. 8 Wear debris in the resulting oil after the friction test using the optimized running-in process of 16 N (3 h) + 64 N (2 h).

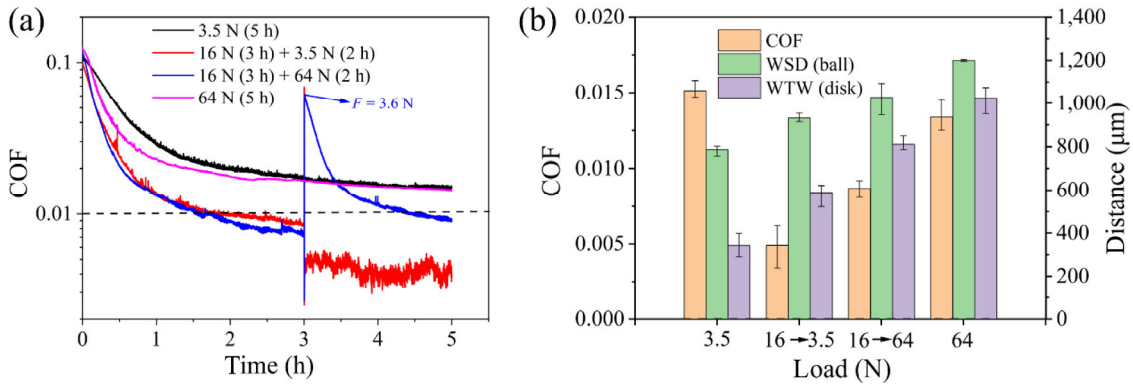

Fig. 7 (a) COF evolution and (b) resulting COF, WSD, and WTW values in the friction tests using optimized running-in processes.

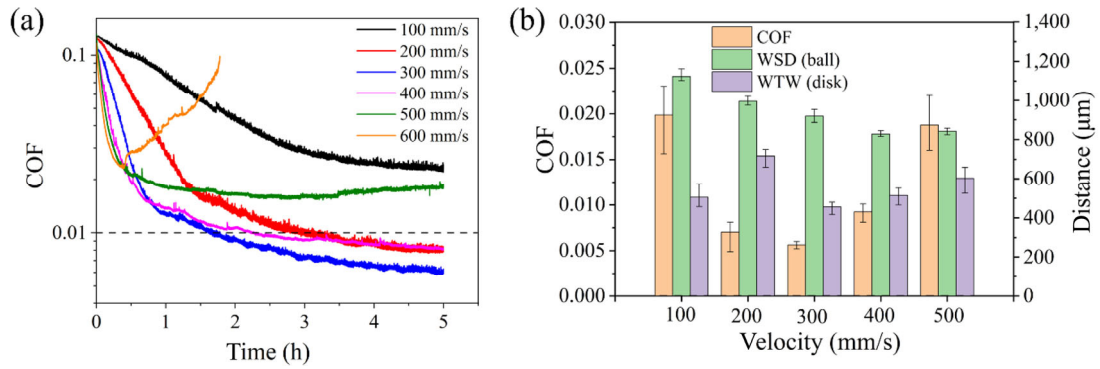

Fig. 9 (a) COF evolution and (b) resulting COF, WSD, and WTW values in the friction tests at various velocities.

stage of the COF stopped within 1 h and gradually rose to 0.02 when the test was finished. The worst lubrication performance was observed at the highest testing velocity of 600 mm/s. After a short-time decrease, the COF sharply increased to 0.1, which was considered as the lubrication failure and the friction test was then terminated. By analyzing the wear scars and wear tracks (Figs. S4 and S5 in the ESM), it is found that the WSD of the ball decreased with the increasing velocity (Fig. 9(b)), since the stronger hydrodynamic effect reduced the wear in the running-in stage, which was dominated in the wear process, but the WTW of the disk did not show monotonic variation with the velocity. This phenomenon was probably due to their different wear rate and wear stage.

Similar to the friction tests under various loads, the tests at various velocities also led to different colors of the resulting oil. As shown in Fig. 10(a), the red color of the resulting oil turned lighter with the increasing velocity, which indicates the lower content of iron complex witnessed by the FTIR spectra (Fig. 10(b)). It should also be noted that oil spreading from the disk center occurred when the velocity was higher than 400 mm/s, in which cases the left oil was too little to be collected for FTIR analysis. This oil migration induced by the strong centrifugal force caused severe oil starvation and lubrication failure at velocities of 600 mm/s.

To make an in depth analysis for the unachievable superlubricity at 100 mm/s, an additional friction test at 100 mm/s with the extended testing time was designed. As the sliding distance at 300 mm/s for 5 h was 5,400 meters, the friction test at 100 mm/s was remeasured for 15 h to reach the identical sliding distance. Figure 11(a) shows that the running-in process continued with the extending sliding distance. By forming better conformity on sliding surfaces (Fig. 11(b) and Fig. S6 in the ESM), a much lower COF of 0.014 was reached but still higher than the superlubricity level. Oil Analysis after the test (Fig. 12) shows that

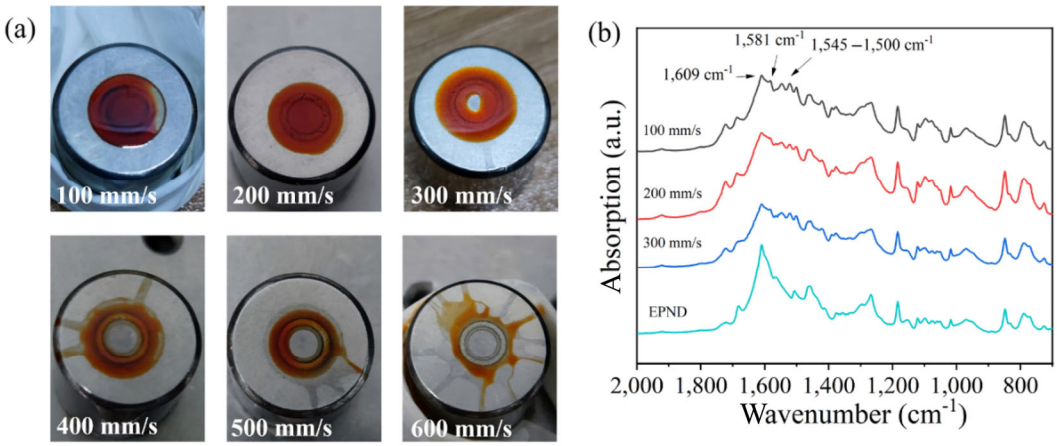

Fig. 10 (a) Photos of the resulting oil on steel disks and (b) FTIR spectra of pure EPND and the resulting oil after the friction tests at various velocities.

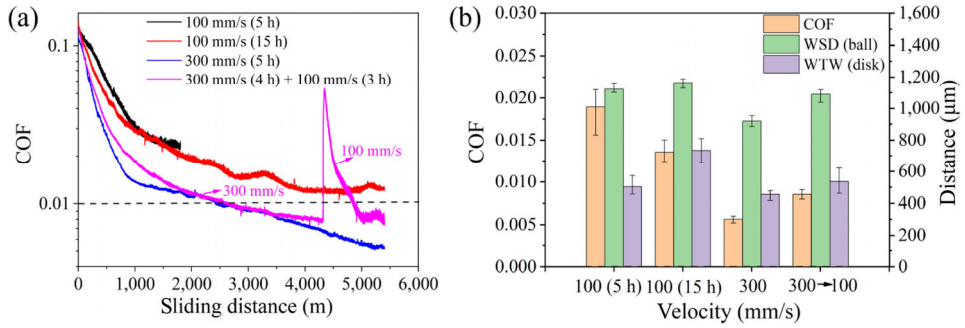

Fig. 11 (a) COF evolution and (b) resulting COF, WSD, and WTW values in the friction tests using optimized running-in processes.

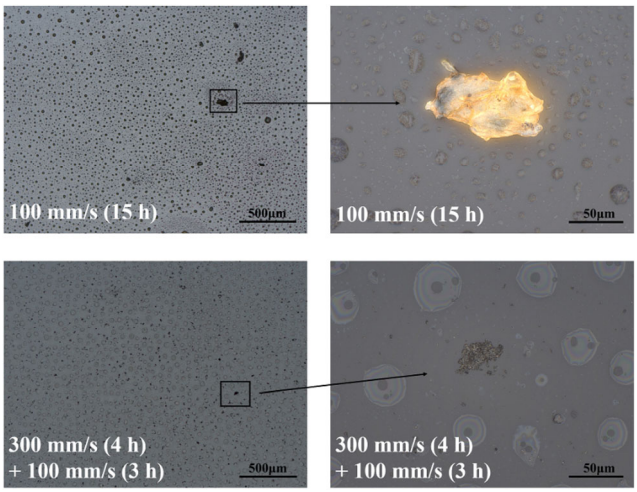

Fig. 12 Wear debris in the resulting oil after the friction tests at 100 mm/s (15 h) and 300 mm/s (4 h) + 100 mm/s (3 h).

abrasive particles with the size over 100 μm were produced, which hindered the further decline of COF. Based on the optimized running-in method used in the friction test under various loads in Fig. 7, a similar two-stage running-in process with different velocities was proposed. The first step was a running-in process at 300 mm/s for 4 h to achieve superlubricity, then the second stage of the test switched the velocity to 100 mm/s for 3 h to ensure the same entire sliding distance of 5,400 meters. The result shows that after a short second-stage running-in process the superlubricity was recovered at 100 mm/s. It is interesting that although the test at 100 mm/s (15 h) has more significant wear and better surface conformity than the two-stage running in process of 300 mm/s (4 h) + 100 mm/s (3 h), the former still exhibits higher COF. This phenomenon can be explained by comparing the amount and the size of wear debris in Fig. 12. As severe mechanical wear always occurs in the high friction stage, the optimized running-in process could avoid the generation of big debris.

3.3 Critical working conditions and superlubricity region

By combining the friction tests of Set 1 and Set 2, Table 1 summarizes all the results on various operating conditions. According to the data of WSD, WTW, WTW/WSD ratio, debris size, and oil retention state, the critical conditions for achieving superlubricity were discussed. (1) Under the low load (3.5 N), due to the insufficient running-in, it could not form good asperity level conformity between the upper and lower surfaces through a certain amount of wear. (2) Under the high load (64 N), due to the excessive frictional force, severe collisions between surface asperities produced considerable wear debris (> 200 μm) that hindered the achievement of superlubricity. (3) At the low velocity (100 mm/s), even if the testing time was extended to ensure adequate sliding distance, the generated big debris around 100 μm still deteriorated the lubrication performance. It should be noted that particles of the similar size could also be found in the test under 43 N and 300 mm/s with the stable superlubricity performance, indicating that a stronger hydrodynamic effect could tolerate the debris in such size. (4) At the high velocity (500 mm/s), oil migration occurred due to the strong centrifugal force, and resulted in oil starvation in the contact area. Based on these critical operating conditions, a COF map of EPND in the studied lubrication system is proposed in Fig. 13(a). Although the number of tests is limited in this work, it is rational to deduce that the green area can roughly illustrate the superlubricity region in this study.

Table 1 Summarized results of the friction tests on various operating conditions.

Operating condition		WSD (μm)	WTW (μm)	WTW/WSD	Max. Debris size (μm)	Oil migration	Superlubricity
V = 300 mm/s	3.5N (5 h)	786	341	0.43	10	No	No
	8N (5 h)	865	437	0.51	20	No	Yes
	16 N (5 h)	919	456	0.50	20	No	Yes
	27 N (5 h)	1,015	690	0.68	90	No	Yes
	43N (5 h)	1,053	765	0.73	100	No	Yes
	64 N (5 h)	1,199	1,024	0.85	200	No	No
	16 N (3 h) + 3.5 N (2 h)	930	589	0.63	20	No	Yes
	16 N (3 h) + 64 N (2 h)	1,027	810	0.79	30	No	Yes
N = 16 N	100 mm/s (5 h)	1,123	504	0.45	100	No	No
	200 mm/s (5 h)	996	716	0.72	50	No	Yes
	300 mm/s (5 h)	919	456	0.50	20	No	Yes
	400 mm/s (5 h)	829	545	0.66	—	Slight	Yes
	500 mm/s (5 h)	841	603	0.72	—	Severe	No
	100 mm/s (15 h)	1,165	755	0.65	100	No	No
	300 mm/s (4 h) + 100 mm/s (3 h)	1,088	539	0.50	30	No	Yes

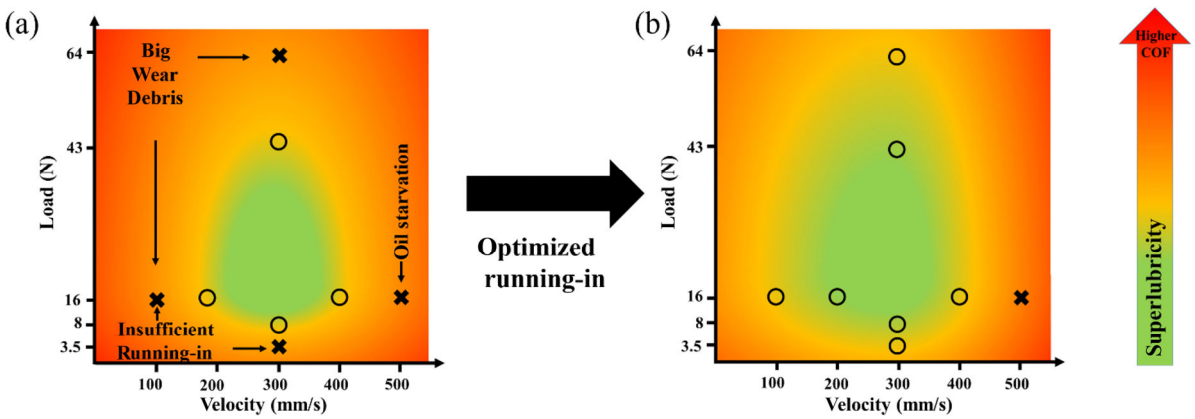

Fig. 13 Superlubricity region of EPND in the studied lubrication system (the symbol "O" and "X" refer to the COF lower or higher than 0.01 respectively).

With the eagerness to apply the superlubricity technique in broader potential fields, this work has also proposed an optimized running-in method to expand the load and velocity boundaries of superlubricity. In the first stage, an optimized operating condition (16 N and 300 mm/s) was set to initiate a suitable running-in process to achieve superlubricity. After that, by reducing/increasing the load or reducing the velocity to the target value within a specific range, the superlubricity performance can be maintained or recovered in a relatively short second-stage running-in. In such a way, the superlubricity region can be expanded (Fig. 13(b)). It is worth noting that the negative influences such as the excessive wear and big wear debris mainly take place in the high friction stage induced by the high load (64 N) or the low velocity (100 mm/s). Once the optimized running-in process avoids those irreversibly deteriorative influences, the superlubricity performance should be very stable even when the load or velocity is switched back. In

fact, our previous works [29, 39] have verified that after EPND reaches superlubricity, its tribochemical reaction can be automatically stopped, and both the tribochemical wear and the mechanical wear are all self-limited within the running-in period. In such a situation, only a drop of EPND, without any oil replenishment or replacement, can maintain the superlubricity for more than 70 h. Therefore, it is supposed that the optimized running-in approach proposed in this study is effective and of long-term benefit.

Moreover, it should be pointed out that the superlubricity region in Fig. 13(b) is only based on the friction tests studied here, which has the potential to be further expanded. For instance, if the target load is higher than 64 N, after the first-stage running-in process, it is still possible to reach superlubricity with a longer second-stage running-in period or with an increased velocity of 400 mm/s simultaneously. In fact, we have already proved that superlubricity under 100 N could be achieved using this method (Fig. S7 in the ESM), which is also the highest load for all reported oil-based superlubricity systems so far. On the other hand, the load and velocity boundaries in Fig. 13(b) may vary by changing the contact situation and movement mode of friction pairs [45], or the oil supplement manner of the lubrication system. For instance, our previous work [12] had already confirmed that at a very high velocity of 1,060 mm/s, EPND could quickly reach superlubricity within 1 h when it kept immersing the friction pairs in an oil bath. Therefore, rather than the exact critical load or velocity values in Fig. 13, the discovered mechanism of superlubricity failure and the proposed approach of expanding the superlubricity region are of greater significance. With a well-designed operating strategy, it is reasonable to imagine that EPND is promising for a wide range of applications in industry.

4 Conclusions

The present work investigated the effect of load and velocity on the superlubricity achievability of 1,3-diketone oil. The results show that the achievement of superlubricity requires a sufficient running-in process to realize surface conformity. Meanwhile, it is necessary to avoid large wear debris and oil starvation during the running-in process. Therefore, the appropriate combination of load and velocity determines the boundary of the superlubricity region. Moreover, based on the discovered superlubricity failure mechanism, this work proposed an optimized running-in method to expand the load and velocity boundaries. To sum up, by clarifying the critical operating conditions, the results of this study are helpful for oil-based superlubricity to seek potential applications, and provide the guidance for utilizing this novel technology more effectively.

Acknowledgements

This work was supported by the National Natural Science Foundation of China (No. 51975437), and the Sino-German Center for Research Promotion (SGC) (GZ 1576).

Electronic Supplementary Material: Supplementary material is available in the online version of this article at https://doi.org/10.1007/s40544-022-0647-0.

References

[1] Hirano M, Shinjo K. Atomistic locking and friction. *Phys Rev B* **41**(17): 11837–11851 (1990)

[2] Shinjo K, Hirano M. Dynamics of friction: Superlubric state. *Surf Sci* **283**(1–3): 473–478 (1993)

[3] Luo J B, Zhou X. Superlubricitive engineering—Future industry nearly getting rid of wear and frictional energy consumption. *Friction* **8**(4): 643–665 (2020)

[4] Tang G, Wu Z, Su F, Wang H, Xu X, Li Q, Ma G, Chu P K. Macroscale superlubricity on engineering steel in the presence of black phosphorus. *Nano Lett* **21**(12): 5308–5315 (2021)

[5] Zheng Z W, Liu X L, Huang G W, Chen H J, Yu H X, Feng D P, Qiao D. Macroscale superlubricity achieved via hydroxylated hexagonal boron nitride nanosheets with ionic liquid at steel/steel interface. *Friction* **10**(9): 1365–1381 (2022)

[6] Ma Q, He T, Khan A M, Wang Q J, Chung Y W. Achieving macroscale liquid superlubricity using glycerol aqueous solutions. *Tribol Int* **160**: 107006 (2021)

[7] Li P P, Ji L, Li H X, Chen L, Liu X H, Zhou H D, Chen J M. Role of nanoparticles in achieving macroscale superlubricity of graphene/nano-SiO_2 particle composites. *Friction* **10**(9): 1305–1316 (2022)

[8] Ma Q, Wang S, Dong G. Macroscale liquid superlubricity achieved with mixtures of fructose and diols. *Wear* **484–485**: 204037 (2021)

[9] Liu S W, Wang H P, Xu Q, Ma T B, Yu G, Zhang C, Geng D, Yu Z, Zhang S, Wang W. Robust microscale superlubricity under high contact pressure enabled by graphene-coated microsphere. *Nat Commun* **8**: 14029 (2017)

[10] Liu W, Wang H, Liu Y, Li J, Erdemir A, Luo J. Mechanism of superlubricity conversion with polyalkylene glycol aqueous solutions. *Langmuir* **35**(36): 11784–11790 (2019)

[11] Cao Y, Kampf N, Lin W, Klein J. Normal and shear forces between boundary sphingomyelin layers under aqueous conditions. *Soft Matter* **16**(16): 3973–3980 (2020)

[12] Amann T, Kailer A, Oberle N, Ke L, Rühe J. Macroscopic superlow friction of steel and diamond-like carbon lubricated with a formanisotropic 1,3-diketone. *ACS Omega* **2**(11): 8330–8342 (2017)

[13] Jia W, Bai P, Zhang W, Ma L, Meng Y, Tian Y. On lubrication states after a running-in process in aqueous lubrication. *Langmuir* **35**(48): 15435–15443 (2019)

[14] Xiao C, Li J, Gong J, Chen L, Zhang J, Qian L, Luo J. Gradual degeneration of liquid superlubricity: Transition from superlubricity to ordinary lubrication, and lubrication failure. *Tribol Int* **130**: 352–358 (2019)

[15] Zhang S, Zhang C, Chen X, Li K, Jiang J, Yuan C, Luo J. XPS and ToF-SIMS analysis of the tribochemical absorbed films on steel surfaces lubricated with diketone. *Tribol Int* **130**: 184–190 (2019)

[16] Xiao C, Li J, Chen L, Zhang C, Zhou N, Qian L, Luo J. Speed dependence of liquid superlubricity stability with H_3PO_4 solution. *RSC Adv* **7**(78): 49337–49343 (2017)

[17] Ge X, Li J, Wang H, Zhang C, Luo J. Macroscale superlubricity under extreme pressure enabled by the combination of graphene-oxide nanosheets with ionic liquid. *Carbon* **151**: 76–83 (2019)

[18] Deng M, Li J, Zhang C, Ren J, Zhou N, Luo J. Investigation of running-in process in water-based lubrication aimed at achieving super-low friction. *Tribol Int* **102**: 257–264 (2016)

[19] Li K, Amann T, List M, Walter M, Moseler M, Kailer A, Rühe J. Ultralow friction of steel surfaces using a 1,3-diketone lubricant in the thin film lubrication regime. *Langmuir* **31**(40): 11033–11039 (2015)

[20] Li J, Zhang C, Luo J. Superlubricity achieved with mixtures of polyhydroxy alcohols and acids. *Langmuir* **29**(17): 5239–5245 (2013)

[21] Chen Z, Liu Y, Zhang S, Luo J. Controllable superlubricity of glycerol solution via environment humidity. *Langmuir* **29**(38): 11924–11930 (2013)

[22] Li J, Zhang C, Deng M, Luo J. Investigation of the difference in liquid superlubricity between water- and oil-based lubricants. *RSC Adv* **5**(78): 63827–63833 (2015)

[23] Li J, Zhang C, Luo J. Superlubricity behavior with phosphoric acid-water network induced by rubbing. *Langmuir* **27**(15): 9413–9417 (2011)

[24] Li J, Ma L, Zhang S, Zhang C, Liu Y, Luo J. Investigations on the mechanism of superlubricity achieved with phosphoric acid solution by direct observation. *J Appl Phys* **114**(11): 10583 (2013)

[25] Deng M M, Zhang C H, Li J J, Ma L R, Luo J B. Hydrodynamic effect on the superlubricity of phosphoric acid between ceramic and sapphire. *Friction* **2**(2): 173–181 (2014)

[26] Jiang Y, Xiao C, Chen L, Li J, Zhang C, Zhou N, Qian L, Luo J. Temporary or permanent liquid superlubricity failure depending on shear-induced evolution of surface topography. *Tribol Int* **161**: 107076 (2021)

[27] Meng Y G, Xu J, Jin Z M, Prakash B, Hu Y Z. A review of recent advances in tribology. *Friction* **8**(2): 221–300 (2020)

[28] Amann T, Kailer A. Ultralow friction of mesogenic fluid mixtures in tribological reciprocating systems. *Tribol Lett* **37**(2): 343–352 (2010)

[29] Li K, Amann T, Walter M, Moseler M, Kailer A, Rühe J. Ultralow friction induced by tribochemical reactions: A novel mechanism of lubrication on steel surfaces. *Langmuir* **29**(17): 5207–5213 (2013)

[30] Liu D, Li K, Zhang S, Amann T, Zhang C, Yan X. Anti-spreading behavior of 1,3-diketone lubricating oil on steel surfaces. *Tribol Int* **121**: 108–113 (2018)

[31] Li K, Jiang J, Amann T, Yuan Y, Wang C, Yuan C, Neville A. Evaluation of 1,3-diketone as a novel friction modifier for lubricating oils. *Wear* **452–453**: 203299 (2020)
[32] Yang J, Yuan Y, Li K, Amann T, Wang C, Yuan C, Neville A. Ultralow friction of 5CB liquid crystal on steel surfaces using a 1,3-diketone additive. *Wear* **480–481**: 203934 (2021)
[33] Li K, Zhang S, Liu D, Amann T, Zhang C, Yuan C, Luo J. Superlubricity of 1,3-diketone based on autonomous viscosity control at various velocities. *Tribol Int* **126**: 127–132 (2018)
[34] Wen Y Q, Tang J Y, Zhou W, Li L, Zhu C C. New analytical model of elastic-plastic contact for three-dimensional rough surfaces considering interaction of asperities. *Friction* **10**(2): 217–231 (2022)
[35] Chen Z, Liu Y, Luo J. Superlubricity of nanodiamonds glycerol colloidal solution between steel surfaces. *Colloids Surf A Physicochem Eng Aspects* **489**: 400–406 (2016)
[36] Wang W, Wong P L, Zhang Z. Experimental study of the real time change in surface roughness during running-in for PEHL contacts. *Wear* **244**(1): 140–146 (2000)
[37] Ram Tyagi M, Sethuramiah A. Asperity level conformity in partial EHL Part I: Its characterization. *Wear* **197**(1): 89–97 (1996)
[38] Ram Tyagi M, Sethuramiah A. Asperity level conformity in partial EHL Part II—Its influence in lubrication. *Wear* **197**(1): 98–104 (1996)
[39] Amann T, Kailer A. Analysis of the ultralow friction behavior of a mesogenic fluid in a reciprocating contact. *Wear* **271**(9–10): 1701–1706 (2011)
[40] Xu J, Kato K. Formation of tribochemical layer of ceramics sliding in water and its role for low friction. *Wear* **245**(1–2): 61–75 (2000)
[41] Gates R S, Hsu S M. Tribochemistry between water and Si_3N_4 and SiC: Induction time analysis. *Tribol Lett* **17**(3): 399–407 (2004)
[42] Andersson J, Larsson R, Almqvist A, Grahn M, Minami I. Semi-deterministic chemo-mechanical model of boundary lubrication. *Faraday Discuss* **156**: 343 (2012)
[43] Tysoe W. On Stress-induced tribochemical reaction rates. *Tribol Lett* **65**(2) : 48 (2017)
[44] Wen X, Bai P, Li Y, Cao H, Li S, Wang B, Fang J, Meng Y, Ma L, Tian Y. Effects of abrasive particles on liquid superlubricity and mechanisms for their removal. *Langmuir* **37**(12): 3628–3636 (2021)
[45] Tortora A M, Halenahally Veeregowda D. Effects of two sliding motions on the superlubricity and wear of self-mated bearing steel lubricated by aqueous glycerol with and without nanodiamonds. *Wear* **386-387**: 173–178 (2017)

Yuyang YUAN. He joined Reliability Engineering Institute, National Engineering Research Center for Water Transport Safety, at Wuhan University of Technology, as a master student since 2019. He is now focusing on the studies about oil-based superlubricity.

Ke LI. He received his B.S. and M.S. degrees in materials science from Wuhan University of Technology in 2007 and 2010, and the Ph.D. degree in microsystem engineering from University of Freiburg, Germany, in 2014, respectively. Then he joined the National Engineering Research Center for Water Transport Safety at Wuhan University of Technology. His current position is a professor, and his research mainly focuses on oil-based superlubricity and ecofriendly lubricants.